Bonding trends in the group-IV*A* dimers C_2-Pb_2

J. Harris* and R. O. Jones
Institut für Festkörperforschung der Kernforschungsanlage Jülich, D-5170 Jülich, Germany
(Received 14 November 1978)

Energy curves have been calculated for low-lying states on Sn_2 and Pb_2 by means of the density-functional formalism. Remarkably similar results can be obtained by representing the core by a simple local pseudopotential. With these and our earlier results for C_2-Ge_2, trends in this series are discussed, with particular reference to the tails of the atomic s- and p-valence functions. An immediate consequence is an understanding of the special nature of the C-C bond.

I. INTRODUCTION

In previous papers,[1,2] we have reported density-functional (DF) and pseudodensity-functional (PDF) calculations of the energy curves of the group-IV dimers Si_2 and Ge_2. The present work extends these calculations to the remaining members of the group-IV*A* dimers Sn_2 and Pb_2, discusses the use of a local pseudopotential to represent the effects of the nucleus and core electrons, and details binding trends from C_2–Pb_2. In particular, the low-lying states of Si_2–Pb_2 are remarkably similar. In each molecule, the ground state is $^3\Sigma_g^-(\pi_u^2 2\sigma_g^2)$, the level ordering is almost identical, and, apart from differences arising from the different nuclear masses, the spectroscopic constants are very similar. These features and the exceptional nature of C_2 can be understood in terms of the tails of the atomic valence orbitals (Sec. IV).

Both Sn_2 and Pb_2 have a large number of core electrons, which we treat as detailed previously.[3] The density of inner-core electrons is frozen, and the outer core, while remaining unpolarized, is allowed to adjust to changes in the molecular potential. This procedure breaks down when core overlap is substantial, because the valence and core orbitals are no longer orthogonal.[3] To circumvent this problem, we have repeated all calculations using the pseudodensity-functional,[1] where the core and nucleus are replaced by a fixed local potential. Criteria for choosing the potential and the actual potentials used for Sn and Pb are given in Sec. II. Results of DF and PDF calculations for low-lying states of Pb_2 and Sn_2 are given in Sec. III. The correspondence between the two sets of results is close, and supports use of the PDF for larger systems where extended cores may give rise to difficulties. Bonding trends are discussed in Sec. IV, together with available experimental data. The calculated binding energy for Pb_2 is greater than the mass-spectrometric estimate, which makes this dimer unique among the sp-bonded systems we have considered.

II. PSEUDOPOTENTIALS FOR Sn AND Pb

The DF and PDF give similar results for energy differences in Si and Si_2,[1] provided that the pseudoorbitals arising from $V_{ps}^{ext}(r)$ and the atomic valence orbitals show maximum agreement outside the core region This criterion has also been used by other authors,[4] and Starkloff and Joannopoulos[5] have shown that a smoothed empty-core potential of the form

$$V_{ps}^{ext}(r) = \frac{-2Z_v}{r} \frac{1-\exp(-\lambda r)}{1+\exp\lambda(r_c-r)}, \tag{1}$$

where Z_v is the valence charge, provides a reasonable tail fit for a variety of atoms. An important feature of (1) is that, for large λ, it attains rapidly the correct form $-2Z_v/r$ for $r \gg r_c$. For Ge, a single choice of r_c gives a satisfactory tail fit for both s and p functions, but this is not generally so and it is necessary to introduce either an l-dependent pseudopotential or an additional potential $V'(r)$ which shifts the s orbital relative to the p. The outward shift necessary in Si could be achieved by adding a repulsive spike peaked at the origin. For Sn and Pb, a shift in the opposite direction is required, and the following pseudopotentials were found to give a satisfactory tail fit:

$$\begin{aligned} &\text{Sn: } \lambda = 16, \quad r_c = 1.33, \quad V' = -85(0.5 - r)\theta(0.5 - r), \\ &\text{Pb: } \lambda = 14, \quad r_c = 1.51, \quad V' = -8(1 - r/r_c)\theta(r_c - r), \end{aligned} \tag{2}$$

where $\theta(x)$ is zero for $x > 0$ and unity otherwise.

Comparison with the true valence eigenfunctions is shown in Fig. 1, where it is evident that the pseudotails do not peak sharply enough for $r \gtrsim r_c$.

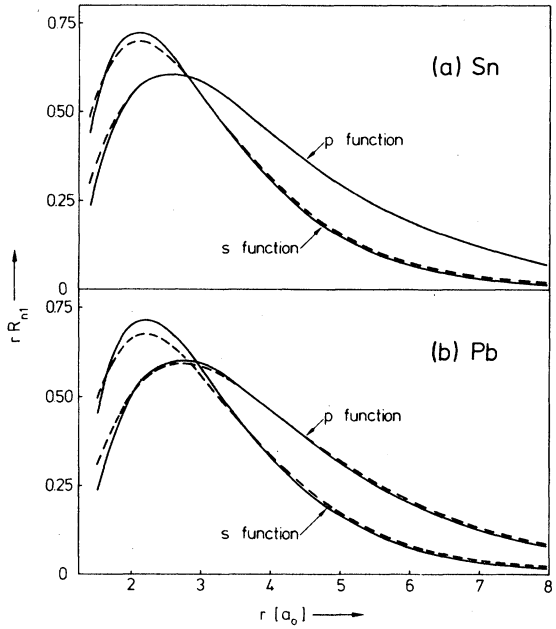

FIG. 1. Tails of pseudo-wave-functions (broken curves) and atomic valence functions (full curves) for (a) Sn and (b) Pb.

A pseudopotential with an explicit l dependence would certainly lead to improved agreement, but the fit (Fig. 1) is adequate for present purposes.

Tables I and II show atomic eigenvalues, ionization energies, and s-p promotion energies as given by the DF and PDF. The agreement is generally good, though the s-p promotion energies given by the pseudofunctional are too small. This error is due to two effects. First, the pseudopotential eigenvalues ϵ_s^{ps} lie too high (note that the s tail is not well fitted in either case), and second, the spin energy given by the two functionals is different. The spin energy is larger in the PDF because it is an increasing function of the spin polarization[6] (the ratio of the spin density to the total density), which is larger in the absence of core electrons. Changes in density and spin density on dimer formation are much smaller than in the $s^2p^2 \rightarrow s^1p^3$ transition, and better agreement between DF and PDF results can be expected. The ionization energies, where the s eigenvalue and s spin are not involved, are given much more accurately by the PDF.

TABLE I. Eigenvalues ϵ_i and excitation energies ΔE for atomic configurations of Sn (Ry). Values with superscript are from the pseudodensity functional; others are from the full functional.

	Sn ($5s^25p^2$)	Sn ($5s5p^3$)	Sn^+ ($5s^25p$)
ϵ_{5s}	−0.755	−0.810	−1.274
ϵ_s^{ps}	−0.715	−0.770	−1.243
ϵ_{5p}	−0.302	−0.343	−0.781
ϵ_p^{ps}	−0.300	−0.340	−0.783
ΔE	...	0.322	0.568
ΔE^{ps}	...	0.224	0.567

TABLE II. Eigenvalues ϵ_i and excitation energies ΔE for atomic configurations of Pb (Ry). Values with superscript are from the pseudodensity functional; others are from the full functional.

	Pb ($6s^26p^2$)	Pb ($6s6p^3$)	Pb^+ ($6s^26p$)
ϵ_{6s}	−0.730	−0.783	−1.241
ϵ_s^{ps}	−0.679	−0.735	−1.181
ϵ_{6p}	−0.297	−0.336	−0.764
ϵ_p^{ps}	−0.288	−0.327	−0.746
ΔE	...	0.316	0.551
ΔE^{ps}	...	0.212	0.542

III. BINDING-ENERGY CURVES FOR Sn_2 AND Pb_2

Binding-energy curves for six low-lying configurations of Sn_2 and Pb_2 are shown in Figs. 2 and 3, respectively. All states have a fully occupied 1σ shell and partial occupancy of π_u, $2\sigma_g$, and π_g orbitals ($^3\Sigma_g^-$, $^1\Sigma_g^+$, $^1\Delta_g : \pi_u^2 2\sigma_g^2$; $^3,{}^1\Pi_u : \pi_u^3 2\sigma_g^1$; $^1\Sigma_g^+ : \pi_u^4$; $^5\Pi_g : \pi_u^2 2\sigma_g^1 \pi_g^1$). Both DF and PDF results are given and, to aid comparison, the separations at which the DF results cease to be reliable due to orthogonality errors (5.2 a_0 for Sn_2 and 5.4 a_0 for

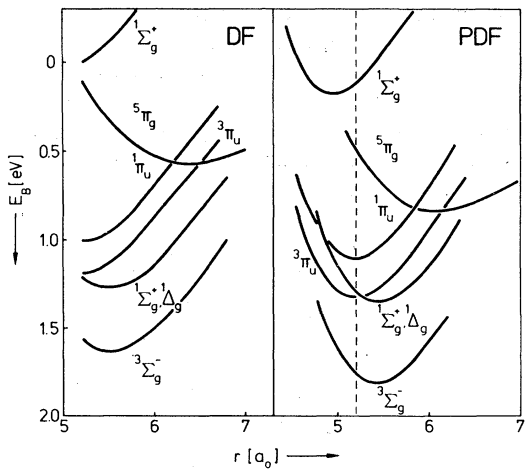

FIG. 2. Energy curves for low-lying states of Sn_2 calculated by means of the density functional (DF) and pseudo-density functional, (PDF). The broken vertical line is to aid comparison between the two sets of curves (see text).

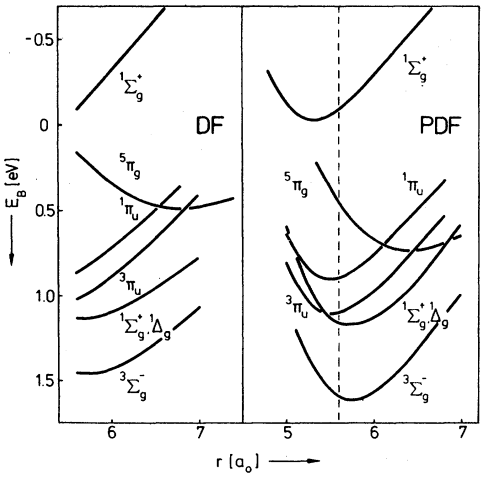

FIG. 3. Energy curves for low-lying states of Pb_2 calculated by means of the density functional (DF) and pseudodensity functional (PDF). The broken vertical line is to aid comparison between the two sets of curves (see text).

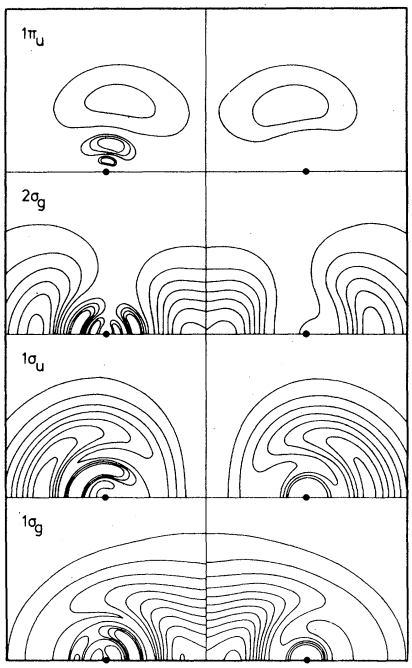

FIG. 4. Valence-orbital densities for $^3\Sigma_g^-$ state of Sn_2 for $r_e = 5.4\ a_0$. Left-hand side: DF results, with bond center at the lower-right-hand side of each frame. Right-hand side: PDF results with bond center at the lower-left-hand side of each frame to aid comparison with the DF results. Contour interval is $0.002 e a_0^{-3}$, except for the $2\sigma_g$ orbital, where it is $0.004 e a_0^{-3}$. For reasons of clarity, contours are not plotted in particularly dense regions, e.g., near the nuclei.

Pb_2) are shown (dashed line). The spectroscopic constants in Table III are calculated by means of the DF energies where these values were sufficiently complete, otherwise the PDF results were used. The correspondence between DF and PDF results is clear, the main difference being an overall shift to higher binding energies in the latter (~0.2 eV). In accordance with the discussion in Sec. II, singlet-triplet splittings tend to be larger in the PDF.

The pseudopotential (1) is constructed to give the same densities and pseudodensities outside the core of the atom, and it is plausible that the corresponding orbital densities in the dimer should be very similar. This similarity is illustrated in Fig. 4 for the ground state ($^3\Sigma_g^-$) of Sn_2. Although some differences are apparent, they are certainly minor. As noted in Ref. 1, PDF energy curves are sensitive to the choice of pseudopotential. For example, the best fit with a two-parameter potential of the form (1) was found for $\lambda = 6$ and $r_c = 1.18\ a_0$. The resultant pseudofunctions decay more rapidly than the atomic functions for larger r and, in accordance with our earlier experience,[1] lead to an equilibrium separation ($5.28\ a_0$) which is significantly shorter than our three-parameter PDF value ($5.41\ a_0$).

Although there have been several mass-spectro-

TABLE III. Calculated spectroscopic constants for Sn_2 and Pb_2 (see Figs. 2 and 3 and text). Asterisks denote PDF values.

	Sn_2			Pb_2		
	E_B (eV)	$r_e(a_0)$	ω_e (cm^{-1})	E_B (eV)	$r_e(a_0)$	ω_e (cm^{-1})
$^3\Sigma_g^-$	1.64	5.52	175*	1.46	5.72	120*
$^1\Sigma_g^+$, $^1\Delta_g$	1.26	5.52	175*	1.13	5.70	125*
$^3\Pi_u$	1.20	5.18*	180*	1.03	5.52*	130*
$^1\Pi_u$	1.02	5.18*	180*	0.90	5.50*	130*
$^5\Pi_g$	0.57	6.37	90	0.48	6.72	60 65*
$^1\Sigma_g^+$	0.18*	4.95*	190*	0.00*	5.28*	145*

metric investigations of Sn_2,[7,8] there are to our knowledge no band-spectroscopic data which allow the low-lying states to be identified. Our calculations show the ground state to be $^3\Sigma_g^-$, and the calculated binding energy (1.63 eV) shows an underestimate of the measured dissociation energy [1.99 ± 0.17,[7] 1.98 ± 0.18 (Ref. 8)] which is typical of our results for *sp*-bonded systems. Optical data are available for low-lying states[9] of free Pb_2 and for the ground state of the matrix-isolated molecule.[10] The ground-state vibration frequencies (119.1 and 112.2 cm^{-1}, respectively) are in reasonable agreement with the value calculated by means of the PDF (120 cm^{-1}).[11] Other vibration frequencies in Table III may be correlated with measured values for excited states [122,[10] 130,[10] and 162 cm^{-1} (Refs. 9 and 10)], but more work is needed before a detailed assignment can be made. The mass-spectrometric estimate of the dissociation energy of Pb_2 (0.84 ± 0.06 eV)[12] is significantly lower than the calculated value (1.45 eV), this being the only case where the present method has given too large a value in an *sp*-bonded system. This error may be due to our neglect of relativistic corrections to the binding energy. Relativistic Hartree-Fock calculations[13] for CH_4-PbH_4 suggest that the latter are small and tend to increase the calculated binding energy. Relativistic density-functional calculations[14] show, however, that nonrelativistic calculations underestimate *s*-*p* and, in particular, *s*-*d* transfer energies in the Pb atom. The relativistic contraction of the innermost *s* and *p* shells is propagated by orthogonality constraints to the valence orbitals, and leads in turn to improved shielding of the nuclear potential felt by the *d* and *f* electrons.[15] These effects lead to a cohesive energy in lead which is lower than expected from an extrapolation of other group-IV*A* values and, in the present case, would lead to a lower binding energy and shorter equilibrium internuclear separation.

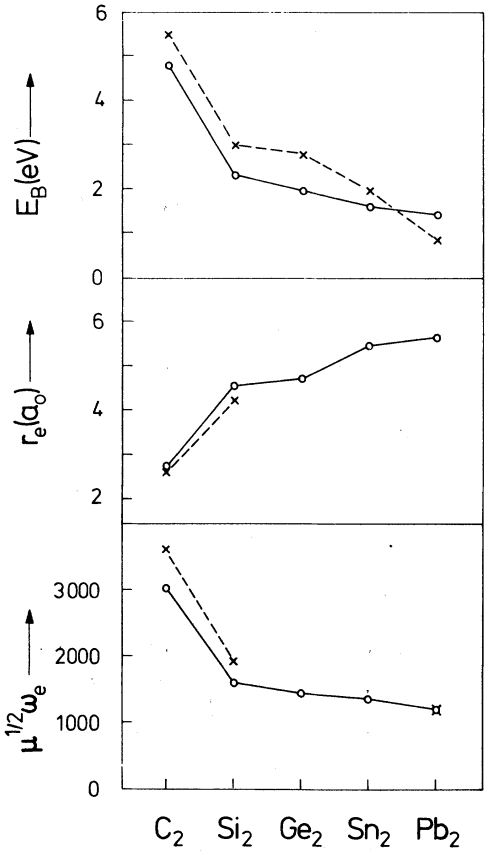

FIG. 5. Binding energies (E_B), equilibrium internuclear separations (r_e), and weighted vibration frequencies ($\mu^{1/2}\omega_e$, where μ is the reduced mass in atomic-weight units and ω_e is in cm^{-1}) for group-IV*A* dimers, Circles represent DF results, with the exception of vibration frequencies for Sn_2 and Pb_2, for which the PDF values given are probably greater than the DF results (see text). Crosses are experimental values: C_2, Ref. 15; Si_2 and Ge_2, see Ref. 2; Sn_2, Ref. 8; Pb_2, Refs. 9 and 12.

IV. BINDING TRENDS IN GROUP IV*A* DIMERS

Spectroscopic constants for the $^3\Sigma_g^-$ state of each dimer are shown in Fig. 5, together with available data. As in the case of the alkali dimers,[16] the observed trend follows closely the behavior of the atomic-orbital tails, with more compact tails leading to stronger binding, smaller r_e, and larger ω_e. In particular, the value of r_e corresponds quite closely to the point where the final antinode in the atomic orbitals is at the bond center (see Fig. 6). This is physically reasonable, since further decrease of the internuclear separation would tend to deplete the charge in the bonding region rather than add to it, even if the configuration is "bonding."

The connection between the molecular binding-energy curve and the atomic-orbital tails is made more transparent on appeal to the Hellmann-Feynman theorem obeyed by the pseudodensity functional. Let $\Delta V_{ps}^{ext}(\vec{r})$ be the change in the molecular pseudopotential consequent on reduction of the internuclear separation from R by a small amount ΔR. Then, since the functional is stationary with respect to changes in the density, the resultant change in the energy is

$$\Delta E(R) = \int d\vec{r}\, n_R(\vec{r})\, \Delta V_{ps}^{ext}(\vec{r}) + \Delta E_N^R, \qquad (3)$$

where $n_R(\vec{r})$ is the molecular density at separation R and where the final term is due to the internuclear repulsion of the cores. For a bonding

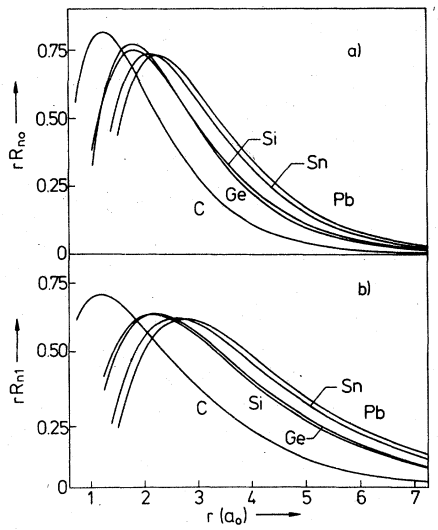

FIG. 6. Tails of valence orbitals for group-IV*A* atoms: (a) *s* functions and (b) *p* functions.

configuration the first term is negative because there are more electrons in the "bonding" region, where $\Delta V_{ps}^{\text{ext}}$ is negative. As the internuclear separation decreases, the magnitude of $\Delta V_{ps}^{\text{ext}}$ increases and ΔE remains negative until a point is reached where the tails from one atomic orbital protrude beyond the second nucleus, adding to the charge in the antibonding region and decreasing the magnitude of the first term in (3) with respect to the second. As the final antinode of the atomic functions reaches the bond center, the attractive force weakens rapidly and ΔE becomes positive. The sooner this occurs, the smaller the value of the binding energy

$$E_B = -\int_{\infty}^{r_e} dR\, \frac{\Delta E(R)}{\Delta R},$$

since the magntiude of $\Delta V_{ps}^{\text{ext}}(\vec{r})$ increases monotonically with decreasing R.

This link between the atomic-orbital tails (Fig. 6) and the molecular binding-energy curves accounts for the trends apparent in Fig. 5, in particular, for the breaks in trend between C_2–Si_2 and Ge_2–Sn_2. Because the atomic orbitals of carbon are particularly compact C_2 binds strongly, while the break between Ge_2 and Sn_2 is clearly related to the irregular behavior of the orbital tails down the group. The origin of this behavior was pointed out by Austin and Heine.[17] As the atomic number increases, the tails are pushed outwards by the requirement of orthogonality to the core, but then relax inward because of the imperfect screening of the nucleus by the extra core shell. Going from Si to Ge this latter effect is particularly marked because of the additional 3*d* core, which is weakly bound and contributes no outward movement to the *s*- and *p*-valence orbitals. The effect is so marked for Ge that outside the core the 4*s* orbital lies inside the 3*s* tail of Si, in spite of the fact that it contains one extra node. The 4*f* shell plays a similar role in drawing the Pb tails towards those of Sn.

Having considered overall trends in binding-energy parameters, we now turn to differences in the multiplet structure, and focus in particular on the energetic separation of the $\pi_u^4: {}^1\Sigma_g^+$ and the $2\sigma_g^2\pi_u^2: {}^3\Sigma_g^-$ molecular states. Calculations reported here and earlier show that the dimers Si_2–Pb_2 have a similar multiplet structure. The ground state is ${}^3\Sigma_g^-$, and the ${}^1\Sigma_g^+$ state mentioned above lies ~1.5 eV higher in energy in each case. The dimer C_2, on the other hand, is exceptional. The calculated ground state is $2\sigma_g^1\pi_u^3: {}^3\Pi_u$, and the $\pi_u^4: {}^1\Sigma_g^+$ and $2\sigma_g^2\pi_u^2: {}^3\Sigma_g^-$ states have about the same energy and lie ~0.6 eV higher.[18] Experimentally, the situation is slightly different, ${}^1\Sigma_g^+$ and ${}^3\Pi_u$ being almost degenerate, with ${}^3\Sigma_g^-$ lying ~0.7 eV higher.[19] This indicates that the functional underestimates the energy of π-bonded configurations, and we may expect the same to be true in the remaining dimers. The error may arise from inadequacies of the basis set or from a general tendency of the functional to underestimate the correlation energy of spreadout charge densities. Nevertheless, it is unlikely to account for the qualitative difference between C_2 and the remaining dimers with respect to the relative positions of the ${}^1\Sigma_g^+$ and ${}^3\Sigma_g^-$ states, and we believe that this separation in $Si_2 \rightarrow Pb_2$ is at least 1 eV.

From the discussion of the relation between molecular energy curves and atomic tails, it is evident that the π_u^4 configuration of C_2 is low-lying, owing to the absence of a *p* core in C and the resultant compactness of the *p* orbital compared with the *s* orbital. In fact, Fig. 6 shows that the final antinode of the C-2*p* orbital lies inside that of the C-2*s*, whereas for the remaining dimers it lies outside. This means that the π orbitals of C_2 are able to concentrate charge in the bonding region as effectively as the σ hybrids, thus accounting for the small energetic separation of the π^4, $\pi^3\sigma^1$, and $\pi^2\sigma^2$ dimer configurations. For the remaining dimers, the *p* orbitals are substantially more extended than their corresponding *s* orbitals, so that the σ charge is stabilized against transfer to the π shell.[20]

To illustrate how these observations correlate with the chemical behavior of C–C and, for example, Si–Si linkages, consider the formation of H–C≡C–H, starting with C≡C in its π_u^4 ground state and bringing the hydrogen atoms from infinity along the molecular axis. The hydrogen atoms interact only with the σ orbitals, leaving

the $\pi\pi$ double bond undisturbed, and, in particular, form strong bonds with the $2\sigma_g$ orbital (see Fig. 4) to give a $1\sigma_g^2 1\sigma_u^2 \pi_u^4 2\sigma_g^2 : {}^1\Sigma_g^+$ ground state. The bond between the carbon atoms is now of increased strength, since the orbitals which bond H to C also bond the carbon atoms to each other. Exactly the same procedure may be followed in the case of Si or another group-IV*A* atom, with the difference that the π_u^4 state of the dimer is unstable by more than 1 eV compared with the $2\sigma_g^2 \pi_u^4$ ground state. In the case of Si, therefore, the addition of two hydrogen atoms leads to a weaker Si–Si bond than in the ground state of the dimer, which explains why H–Si≡Si–H is unstable under normal conditions. In general, the weakness of the π bonds in Si_2–Pb_2 is responsible for their tendency to form only saturated compounds,[21] while the versatility of C_2 in this respect owes its origin to the absence of a p core in the carbon atom.

V. CONCLUDING REMARKS

We have calculated binding-energy curves for the low-lying states of Sn_2 and Pb_2, using the density-functional formalism, and show their ordering to be similar to those of Si_2 and Ge_2 reported earlier. We have demonstrated the connection between the energy curves of a given dimer and the behavior of the atomic-orbital tails, and shown why the multiplet structure of C_2 is different from that of the remaining group-IV*A* dimers. Our calculations are in reasonable agreement with what little data are available for these systems, except for the binding energy of Pb_2, for which our nonrelativistic value exceeds the mass-spectrometric estimate by ~50%. For the most part, however, our calculations are predictions. In addition, we have demonstrated for Sn_2 and Pb_2 that use of the pseudodensity functional, together with a pseudopotential chosen to maximize agreement between the tails of the true atomic valence orbitals and the corresponding pseudoorbitals, leads to results similar to those given by the full density functional. This might be important in performing calculations for larger systems where the presence of large cores and nodal structure in the orbitals can cause numerical complications.

---

*On leave at Metals and Ceramics Division, Oak Ridge National Laboratory, Oak Ridge, Tenn. 37830.

[1]J. Harris and R. O. Jones, Phys. Rev. Lett. 41, 191 (1978).
[2]J. Harris and R. O. Jones, Phys. Rev. A 18, 2159 (1978).
[3]J. Harris and R. O. Jones, J. Chem. Phys. 70, 830 (1979).
[4]S. Topiol, A. Zunger, and M. A. Ratner, Chem. Phys. Lett. 49, 367 (1977); A. Zunger and M. L. Cohen, Phys. Rev. Lett. 41, 53 (1978).
[5]T. Starkloff and J. D. Joannopoulos, Phys. Rev. B 16, 5212 (1977); T. Starkloff, thesis, Universität Mainz, 1977 (unpublished).
[6]O. Gunnarsson and B. I. Lundqvist, Phys. Rev. B 13, 4274 (1976).
[7]M. Ackerman, J. Drowart, F. E. Stafford, and G. Verhaegen, J. Chem. Phys. 36, 1557 (1962), and references therein.
[8]K. A. Gingerich, A. Desideri, and D. L. Cocke, J. Chem. Phys. 62, 731 (1975).
[9]S. E. Johnson, D. Cannell, J. Lunacek, and H. P. Broida, J. Chem. Phys. 56, 5723 (1972).
[10]V. E. Bondybey and J. H. English, J. Chem. Phys. 67, 3405 (1977).
[11]This value is consistent with the general underestimate of vibration frequencies given by the DF in *sp*-bonded systems. Although the DF for Pb_2 data is incomplete (Fig. 3), it is clear that the curvature of the energy curve is less than in the PDF case.
[12]K. A. Gingerich, D. L. Cocke, and F. Miller, J. Chem. Phys. 64, 4027 (1976).
[13]J. P. Desclaux and P. Pyykkö, Chem. Phys. Lett. 29, 534 (1974).
[14]D. Glötzel (private communication).
[15]For a recent discussion of relativistic effects in molecules, see P. Pyykkö, Adv. Quantum Chem. 11, 353 (1978). Relativistic dehybridization of s and p orbitals is noted by J. C. Phillips, *Bonds and Bands in Semiconductors* (Academic, New York, 1973), p. 15.
[16]J. Harris and R. O. Jones, J. Chem. Phys. 68, 1190 (1978).
[17]B. J. Austin and V. Heine, J. Chem. Phys. 45, 928 (1966).
[18]O. Gunnarsson, J. Harris, and R. O. Jones, J. Chem. Phys. 67, 3970 (1977).
[19]E. A. Ballik and D. A. Ramsay, Astrophys. J. 137, 61 (1963); 137, 84 (1963).
[20]The relative ease of s–p transfer in carbon is demonstrated by the trends in $s^2p^2 \rightarrow s^1p^3$ promotion energies for C → Si → Ge. While promotion energies otherwise decrease with increasing atomic number, the calculated values show an increase. Experimental values for C and Si are almost identical and the value for Ge significantly greater [C. E. Moore, *Atomic Energy Levels*, U.S. Natl. Bur. Stand. Circ. No. 467 (U.S. GPO, Washington, D.C., 1949), Vol. I; Vol. II (1952); Vol. III, Appendix (1958)].
[21]For extensive discussions of the Si–Si bond, see *Silicon Chemistry I, II*, edited by F. L. Boschke (Springer, Berlin, 1974), Topics in Current Chemistry, Vols. 50, 51.